Progress In Electromagnetics Research B, Vol. 44, 383–403, 2012

1-D INVERSION OF TRIAXIAL INDUCTION LOGGING IN LAYERED ANISOTROPIC FORMATION

Z. J. Zhang*, N. Yuan, and R. Liu

Well Logging Laboratory, University of Houston, Houston, TX 77204, USA

Abstract—In this paper, we present a one-dimensional (1-D) inversion algorithm for triaxial induction logging tools in multi-layered transverse isotropic (TI) formation. A non-linear least-square model based on Gauss-Newton algorithm is used in the inversion. Cholesky factorization is implemented to improve the stability and the reliability of the inversion. Zero-D inversion is conducted at the center of each layer to provide a reasonable initial guess for the best efficiency of the inversion procedure. Cross components are used to provide sufficient information for determining the boundaries in the initial guess. It will be illustrated that using all the nine components of the conductivity/resistivity yield more reliable inversion results and even faster convergence than using only the diagonal components. The resultant algorithm can be used to obtain various geophysical parameters such as layer boundaries, horizontal and vertical resistivity, dipping angle and rotation angle etc. from triaxial logging data automatically without any priori information. Several synthetic examples are presented to demonstrate the capability and reliability of the inversion algorithm.

1. INTRODUCTION

Electrical anisotropy has been recognized as one potential source of error in traditional induction logging analysis [1]. A common case is a thinly laminated sand-shale sequence where the horizontal resistivity is much smaller than the vertical resistivity. When the well is drilled perpendicular to the bedding planes, conventional induction logging only measures the horizontal resistivity since the tool contain only co-axial transmitter and receiver coils. Thus, the

Received 16 August 2012, Accepted 20 September 2012, Scheduled 5 October 2012

* Corresponding author: Zhi Juan Zhang (zzhijuan@yahoo.com).

interpretation based on the measured data will either miss the pay-zone or overestimate the water saturation [2]. The emerging triaxial induction tool comprises three mutually perpendicular transmitters and three mutually perpendicular receivers along the x, y and z direction. By collecting sufficient information from multiple directions, the triaxial induction tool is capable of detecting formation anisotropy.

For accurate interpretation of the measured data, an efficient inversion procedure is crucial. Via inversion, we can retrieve various geophysical parameters of the formation, such as location of the boundaries, resistivity of each layer, the dipping angle etc. Then petrophysicists are able to evaluate the hydrocarbon content and water saturation based on these parameters. Nowadays, most inversion algorithms are based on one-dimensional (1-D) modeling for the best efficiency since the inversion process requires carrying out the forward modeling repeatedly and thus is usually time consuming [3]. Yu et al. developed an 1-D inversion algorithm based on turbo boosting proposed by Hakvoort [4]. This method describes layered formation using equally thick thin layers with known relative dipping angle and azimuthal angle. In order to stabilize the process, dual frequency data were used. Lu and Alumbaugh [5] performed a new 1-D inversion algorithm using the method of singular value decomposition (SVD) without calculating the sensitivity matrix. However, robust layer position must be known as priori information. Later, Zhang et al. presented three analytical methods for the determination of the relative dipping angle and azimuthal angle [6]. Wang et al. introduced an 1-D inversion algorithm by applying Gauss-Newton to retrieve the transverse isotropic formation parameters [7]. But in this algorithm, initial guess must be determined with some prior information. Recently, Abubakar et al. [8] and Davydycheva et al. [9] developed a three-dimensional (3-D) inversion for triaxial induction logging based on a fully anisotropic 3-D finite-difference forward modeling. The inversion is based on a constrained, regularized Gauss-Newton minimization scheme proposed by Habashy and Abubakar [10]. This inversion algorithm is very robust in extracting formation and invasion anisotropic resistivities, invasion radii, bed boundary locations, relative dip, and azimuth angle from logging data. However, as a full 3-D inversion, the CPU time is still the bottleneck although a dual grid approach was used to speed up the inversion procedure to some extent.

In this paper, we present a 1-D inversion algorithm based on the Gauss-Newton algorithm. Note that we apply Cholesky factorization to update the Hessian matrix from the Gauss-Newton algorithm. Therefore, we are able to improve the reliability and stability of the inversion. Additionally, in our inversion, we employ a Zero-D

inversion which is conducted at the center of each layer to provide a reliable initial model. The efficiency of the entire inversion procedure can be definitely improved if a good initial guess is applied. In the inversion procedure, our previously developed 1-D analytical forward modeling [11] is used as the embedded forward engine. As a result, the developed 1-D inversion algorithm can simultaneously determine the horizontal resistivity, vertical resistivity, formation dip, azimuthal angle and bed boundary position from the triaxial induction logging data. The biggest advantage of the present algorithm is that no priori information is required. Synthetic examples will be presented to illustrate the robustness of the algorithm. We apply the noise in terms of the field noise property into the synthetic data for further testing. Additionally, we compare the efficiency between applying the full triaxial responses and the diagonal terms respectively in the synthetic examples.

2. THEORY

2.1. Triaxial Tool Configuration

A basic triaxial induction tool comprises three pairs of transmitters and receivers oriented at the x, y, and z direction, respectively, as shown in Fig. 1(a). Since the transmitter and receiver coils are infinitely small, we can treat them as magnetic dipoles. The equivalent dipole model is shown in Fig. 1(b). Thus, the magnetic source excitation of the triaxial tool can be expressed as $\mathbf{M} = (M_x, M_y, M_z)\delta(\mathbf{r})$.

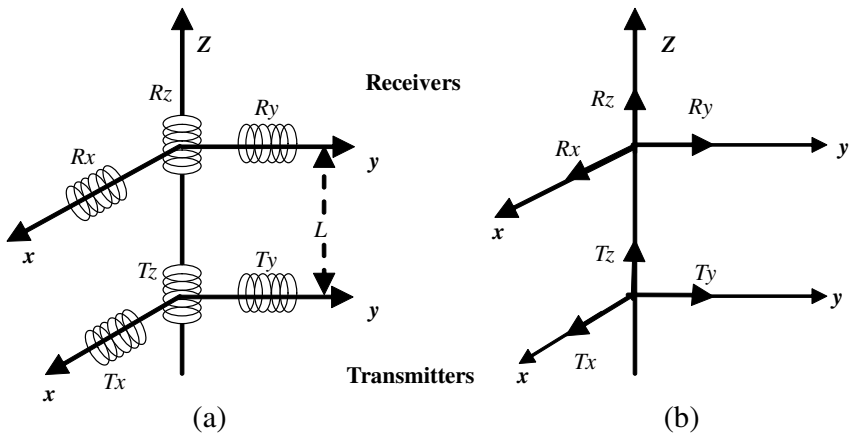

Figure 1. Basic structure of a triaxial induction tool. (a) The original model. (b) The equivalent model.

The tool is moving along the axis in the borehole and for each logging point, a 3×3 apparent conductivity tensor σ_a is measured at each pair of transmitter-receiver spacing, i.e.,

$$\sigma_a = \begin{bmatrix} \sigma_{ax}^x & \sigma_{ax}^y & \sigma_{ax}^z \\ \sigma_{ay}^x & \sigma_{ay}^y & \sigma_{ay}^z \\ \sigma_{az}^x & \sigma_{az}^z & \sigma_{az}^z \end{bmatrix}, \tag{1}$$

where σ_{ai}^j is the apparent conductivity measured at the j-directed receiver from the i-directed transmitter.

The apparent conductivity is a function of the formation true conductivity, formation geometry and the sonde system. In the other words, the apparent conductivity is the convolution among the formation function, the source excitation function and the borehole function. Since our focus is the 1-D case, the borehole function can be ignored. Fig. 2 presents the relative position between the sonde system and the formation.

In Fig. 2, the primed coordinate is for the sonde system, while the unprimed coordinate represents the formation. We have shown three transmitters T_x, T_y, T_z and three receivers R_x, R_y, R_z. The symbol α is a dipping angle between the Z axis and the Z' axis. The symbol β is an azimuthal angle between the x axis and the projection of transmitter coils on the X-Y plane. And γ represents a rotation angle that transmitter T_x is deviated from the X' axis. It has been known that in the transverse isotropic formation, the responses have little sensitivity to the azimuthal angle β [12]. Therefore in our inversion,

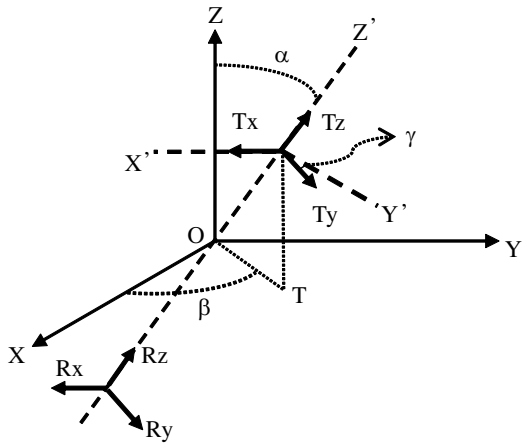

Figure 2. The relationship between tool coordinate and formation coordinate.

we do not have to take account for β. However, we still have to figure out the dipping angle α and the rotation angle γ.

We measure magnetic fields from receivers, as shown (2).

$$\mathbf{H} = \begin{bmatrix} H_x^x & H_x^y & H_x^z \\ H_y^x & H_y^y & H_y^z \\ H_z^x & H_z^y & H_z^z \end{bmatrix}. \tag{2}$$

The magnetics are derived from the Maxwell equations, which involves the Bessel function. In transverse isotropic formation, we assume each formation layer contains a horizontal conductivity and a vertical conductivity. The magnetic fields contain the information of formation conductivity. We can convert the magnetic fields into apparent conductivity by (3).

$$\boldsymbol{\sigma}_a' = \mathbf{K} \cdot \mathbf{H}'. \tag{3}$$

K is the conversion matrix given by tool specific configuration, shown as,

$$\mathbf{K} = \begin{pmatrix} j\frac{8\pi L}{\omega\mu} & j\frac{8\pi L}{\omega\mu} & j\frac{16\pi L}{\omega\mu} \\ j\frac{8\pi L}{\omega\mu} & j\frac{8\pi L}{\omega\mu} & j\frac{16\pi L}{\omega\mu} \\ j\frac{16\pi L}{\omega\mu} & j\frac{16\pi L}{\omega\mu} & j\frac{4\pi L}{\omega\mu} \end{pmatrix}. \tag{4}$$

Although the apparent conductivity is linear to the magnetic fields according to (3), the apparent conductivity is essentially nonlinear to the true conductivity. Therefore we need the nonlinear inversion to extract the true formation parameters.

2.2. Inversion Theory

2.2.1. Gauss-Newton Algorithm

Assume the vector **M** denote the measured conductivity at NR logging points, **M** will be a $9NR\times1$ vector since the conductivity has 9 components at each logging point, i.e.,

$$\begin{aligned} \mathbf{M} &= [m_1, m_2, \ldots, m_{NR}]^T \\ &= \left[\sigma_{x,1}^x, \sigma_{x,1}^y, \sigma_{x,1}^z, \sigma_{y,1}^x, \sigma_{y,1}^y, \ldots, \sigma_{x,NR}^x, \ldots, \sigma_{z,NR}^z\right]^T \end{aligned} \tag{5}$$

In the framework of the inversion, these measured data is assumed to be borehole corrected but with the invasion effect ignored.

In the 1-D inversion model, each layer is characterized by its horizontal conductivity, vertical conductivity and the bed boundary position, yielding a total of $3\times L$-1 parameters for an L-layer formation model. Plus the dipping angle and rotation angle, we will need to

determine $N = 3 \times L + 1$ parameters in the 1-D inversion. Assume the parameter vector $\mathbf{X}$ is the vector composed of the unknown parameters given by

$$\begin{aligned}\mathbf{X} &= [x_1, x_2, \ldots, x_N]^T \\ &= \big[\log(\alpha), \log(\gamma), \log(Z_1), \ldots, \log(Z_{L/3}), \log(\sigma_{h,1}), \ldots, \log(\sigma_{h,L/3}), \\ &\quad \log(\sigma_{v,L/3})\big]^T \end{aligned} \tag{6}$$

All parameters within the proper magnitude range are rescaled due to the application of logarithm. Then we use the parameter vector $\mathbf{X}$ to construct the following objective function (cost function)

$$\mathbf{C}(\mathbf{X}) = \frac{1}{2}\mathbf{R}(\mathbf{X})^{\mathbf{T}} \cdot \mathbf{R}(\mathbf{X}) \tag{7}$$

where $\mathbf{R}(\mathbf{X})$ is the residual function defined by $\mathbf{R}(\mathbf{X}) = \mathbf{S}(\mathbf{X}) - \mathbf{M}$. $\mathbf{S}(\mathbf{X})$ is the simulated tool response corresponding to a particular forward model in terms of the vector $\mathbf{X}$.

As we can see, the cost function measures the error between the calculated log and the input log. The smaller the cost function is, the more reliable inversion results we may obtain. Hence the most critical procedure in the inversion is how to reduce the cost function. We choose the classical nonlinear inversion approach, Gauss-Newton minimization algorithm in our 1-D inversion. According to Taylor expansion, we can approximate the cost function $\mathbf{C}(\mathbf{X})$ with a local quadratic model as follows [13]

$$\begin{aligned}&\mathbf{C}(\mathbf{X}) \\ &\approx \frac{1}{2}\mathbf{R}^{\mathbf{T}}(\mathbf{X}_c)\cdot\mathbf{R}(\mathbf{X}_c) + \mathbf{g}^T(\mathbf{X}_c)\cdot(\mathbf{X}-\mathbf{X}_c) + \frac{1}{2}(\mathbf{X}-\mathbf{X}_c)^T\cdot\bar{\bar{\mathbf{H}}}(\mathbf{X_c})\cdot(\mathbf{X}-\mathbf{X_c})\end{aligned} \tag{8}$$

where $\mathbf{g}(\mathbf{X}) = \nabla\mathbf{C}(\mathbf{X}) = \bar{\bar{\mathbf{J}}}^{\mathbf{T}}(\mathbf{X})\mathbf{R}(\mathbf{X})$ is the gradient of the cost function $\mathbf{C}(\mathbf{X})$ and $\bar{\bar{\mathbf{H}}}(\mathbf{X}) = \nabla\nabla\mathbf{C}(\mathbf{X})$ is the Hessian of the cost function $\mathbf{C}(\mathbf{X})$.

2.2.2. Cholesky Factorization

The Hessian matrix is given by

$$\bar{\bar{\mathbf{H}}}(\mathbf{X}) = \bar{\bar{\mathbf{J}}}^{\mathbf{T}}(\mathbf{X}) \cdot \bar{\bar{\mathbf{J}}}(\mathbf{X}) + \bar{\bar{\mathbf{S}}}(\mathbf{X}) \tag{9}$$

where $\bar{\bar{\mathbf{S}}}(\mathbf{X}) = \sum_{i=1}^{9\times NR} r_i(\mathbf{X})\nabla^2\mathbf{r}_i(\mathbf{X})$ denotes the second-order information in $\bar{\bar{\mathbf{H}}}(\mathbf{X})$. It is not efficient to apply (9) updating the Hessian matrix since (9) also includes the second order information. However, we can take advantage of known information of $J(x)$ to

approximate the Hessian matrix. The approximation can influence the stability of the Hessian matrix. It is important to employ the right approach to get the Hessian matrix. After comparison, we decide to apply Cholesky factorization algorithm and rewrite the Hessian matrix by

$$\bar{\bar{\mathbf{H}}}(\mathbf{X}) = \bar{\bar{\mathbf{J}}}^{\mathbf{T}}(\mathbf{X}) \cdot \bar{\bar{\mathbf{J}}}(\mathbf{X}) + \bar{\bar{\mathbf{S}}}(\mathbf{X}) \approx \bar{\bar{\mathbf{J}}}^{\mathbf{T}}(\mathbf{X}) \cdot \bar{\bar{\mathbf{J}}}(\mathbf{X}) + \mu\mathbf{I} \tag{10}$$

In the inversion, we should notice the sign of the Hessian. The positive Hessian matrix guarantees the final answer is the local minimum. That means the cost function approach to its minimum value. We apply the Cholesky factorization algorithm to update μ in (10). By determining $\mu > 0$, $\bar{\bar{\mathbf{H}}}(\mathbf{X}) \approx \bar{\bar{\mathbf{J}}}^{\mathbf{T}}(\mathbf{X}) \cdot \bar{\bar{\mathbf{J}}}(\mathbf{X}) + \mu\mathbf{I}$ is positive definite, which guarantees the minimum of the cost function to be found. Then (8) can be rewritten as

$$\begin{aligned} \mathbf{C}(\mathbf{X}) \;\approx\; & \frac{1}{2}\mathbf{R}^{\mathbf{T}}(\mathbf{X}_c) \cdot \mathbf{R}(\mathbf{X}_c) + \mathbf{R}^{\mathbf{T}}(\mathbf{X}_c) \cdot \bar{\bar{\mathbf{J}}}(\mathbf{X_c}) \cdot (\mathbf{X} - \mathbf{X_c}) \\ & + \frac{1}{2}(\mathbf{X} - \mathbf{X}_c)^{\mathbf{T}} \cdot \left(\bar{\bar{\mathbf{J}}}^{\,\mathbf{T}}(\mathbf{X_c}) \cdot \bar{\bar{\mathbf{J}}}(\mathbf{X_c}) + \mu\mathbf{I}\right) \cdot (\mathbf{X} - \mathbf{X_c}) \end{aligned} \tag{11}$$

Then the solution of (10) is given by

$$\mathbf{X}_+ \approx \mathbf{X}_c - \left(\bar{\bar{\mathbf{J}}}^{\,\mathbf{T}}(\mathbf{X_c}) \cdot \bar{\bar{\mathbf{J}}}(\mathbf{X_c}) + \mu\mathbf{I}\right)^{-1} \cdot \bar{\bar{\mathbf{J}}}^{\mathbf{T}}(\mathbf{X_c}) \cdot \mathbf{R}(\mathbf{X_c}) \tag{12}$$

2.2.3. The Constrain Algorithm

The Gauss Newton algorithm only gets the global minimum value. However, the parameters have physical meaning. It is necessary to impose a priori maximum and minimum bounds for the unknown parameters. By doing this, we can make sure the inverted parameters are always reasonable. For this purpose, we introduce a nonlinear transformation given by

$$X_i = \frac{x_i^{\max} + x_i^{\min}}{2} + \frac{x_i^{\max} - x_i^{\min}}{2}\sin(c_i), \quad -\infty < c_i < +\infty \tag{13}$$

where $x_i^{\max}$, $x_i^{\min}$ are the upper and lower bounds on the physical model parameter x_i. It is clear that

$$x_i \to x_i^{\min}, \quad \text{as} \;\; \sin(c_i) \to -1 \tag{14}$$

$$x_i \to x_i^{\max}, \quad \text{as} \;\; \sin(c_i) \to +1 \tag{15}$$

Theoretically, by using this nonlinear transformation we should update the artificial unknown parameters c_i instead of the physical model parameters x_i. However, it is straightforward to show that

$$\frac{\partial s_j}{\partial c_j} = \frac{\partial x_i}{\partial c_j}\frac{\partial s_j}{\partial x_i} = \sqrt{\left(x_i^{\max} - x_i\right)\left(x_i - x_i^{\min}\right)}\frac{\partial s_j}{\partial x_i} \tag{16}$$

The two successive iterates $x_{i,k+1}$ and $x_{i,k}$ of x_i are related by

$$\begin{aligned} X_{i,k+1} &= \frac{x_i^{\max}+x_i^{\min}}{2}+\frac{x_i^{\max}-x_i^{\min}}{2}\sin(c_{i,k+1}) \\ &= \frac{x_i^{\max}+x_i^{\min}}{2}+\frac{x_i^{\max}-x_i^{\min}}{2}\sin(c_{i,k}+q_{i,k}) \end{aligned} \tag{17}$$

where

$$c_i = \arcsin\left(\frac{2x_{i,k}-x_i^{\max}-x_i^{\min}}{x_i^{\max}-x_i^{\min}}\right) \tag{18}$$

and $q_{i,k} = c_{i,k+1} - c_{i,k}$ is the Gauss-Newton search step in c_i towards the minimum of the cost functional in (7). This Gauss-Newton direction in x_i is related to the Gauss-Newton direction in c_i through the following relation

$$p_i = q_i \frac{dx_i}{dc_i} \tag{19}$$

Therefore, by applying the relationship in (19) to (17), we obtain the following relationship between the two successive iterates $x_{i,k+1}$ and $x_{i,k}$ of x_i (the step-length γ_k along the search direction x_i is assumed to be adjustable)

$$\begin{aligned} & X_{i,k+1} \\ &= \frac{x_i^{\max}+x_i^{\min}}{2}+\left(x_{i,k}-\frac{x_i^{\max}+x_i^{\min}}{2}\right)\cos\left(\frac{\nu_k p_{i,k}}{\gamma_k}\right)+\gamma_k \sin\left(\frac{\nu_k p_{i,k}}{\gamma_k}\right) \end{aligned} \tag{20}$$

where

$$\gamma_k = \sqrt{(x_i^{\max}-x_{i,k})(x_{i,k}-x_i^{\min})} \tag{21}$$

Thus, in the inversion process there is no need to compute either c_i or q_i explicitly. This will reduce the round-off errors caused by the introduction of the nonlinear function.

2.2.4. Zero-D Inversion

Next, we will describe the choice of the initial model in the inversion procedure since good initial model can significantly improve the efficiency of the inversion. In practical, we do not know the exact number of the layers; therefore we employ a whole space inversion (also called Zero-D inversion) to get the initial model. Zero-D inversion is receiving increasing interest in the study of inversion. Reasonable Zero-D inversion can improve the efficiency of the inversion. Different from the 1-D inversion, the Zero-D inversion inverts parameters based on each logging point. In Zero-D inversion, at each logging point, we should invert four parameters: the dipping angle, rotation angle,

horizontal conductivity and vertical conductivity. In order to be distinguished from the 1-D inversion, the initial guess of the Zero-D inversion is called as starting values. Next, we will explain the choice of the starting values in the zero-D inversion.

Starting Values

In order to get an acceptable starting point for the Zero-D inversion, we use the analytic expressions to compute the dipping angle α and the rotation angle γ horizontal conductivity σ_h and vertical conductivity σ_v directly [6, 14]:

$$\alpha = a\tan\left(\frac{2H^t_{xz\_i}}{H^t_{xx\_i} - H^t_{zz\_i}}\right) \tag{22}$$

$$\gamma = a\tan\left(\frac{2H^c_{xy\_i}}{H^c_{xx\_i} - H^c_{yy\_i}}\right) \tag{23}$$

$$\sigma_h = \frac{4\pi l}{\omega\mu_0}\left[\mathrm{Im}\left(H^{x'}_{x'}\right) + \frac{1}{2}\mathrm{Im}\left(H^{z'}_{z'}\right) + \sqrt{\left(\mathrm{Im}\left(H^{x'}_{x'}\right) - \frac{1}{2}\mathrm{Im}\left(H^{z'}_{z'}\right)\right)^2 + 2\mathrm{Im}\left(H^{x'}_{z'}\right)^2}\right] \tag{24}$$

$$\lambda^2 = 256\pi^2 l^2 \sigma^2_{ha} / \mathrm{Im}\left(H^{z'}_{z'}\right)\left(\mathrm{Im}\left(H^{x'}_{x'}\right) + \mathrm{Im}\left(H^{y'}_{y'}\right) + \mathrm{Im}\left(H^{z'}_{z'}\right) - \frac{\omega\mu_0}{4\pi l}\sigma_h\right) \tag{25}$$

$$\sigma_v = \frac{1}{\lambda^2}\sigma_h \tag{26}$$

where superscripts t and c represent the borehole and the tool coordinates, respectively.

With the aid of the Zero-D inversion, the average values of α, γ are assumed as the initial dipping and rotation angle.

Initial Boundary

After the initial dipping and rotation angle are determined, we need to determine the initial boundary. The common way is to determine the boundary according to the variance of $2\sigma_v - \sigma_h$.

However, this method is instability. As we know, Zero-D inversion results sometimes have large error. Completely relying on the variance based method is 'dangerous'. After sufficient sensitivity analysis and simulation, we have found that the cross components σ_{xz}, σ_{zx} have significant horn effect when the adjacent layers have different horizontal conductivity.

On the other hand, for the layers with close horizontal conductivity, the saddle point always shows the symmetric to the boundary. Hence in this case the middle point can be treated as a

good initial guess to the formation boundary. This is a remarkable finding in determining the formation boundaries. It is more efficient than the variance based method of $2\sigma_v - \sigma_h$ since we can directly detect the boundaries based on cross components.

Therefore, we decide to employ the cross components as a good supplement to determine the initial boundary. In the inversion, we first apply an average filter to eliminate the noise in case computer treated the noise pulse as a boundary. Then we pick up the initial boundaries based on the horn effect of the cross components. Thirdly, the turning points are determined to make sure sufficient boundaries are collected. Finally, we simply merge those initial boundaries in terms of a tolerance. In our inversion, it is 3 ft which matches with the current commercial triaxial tool requirement.

The boundaries are updated after iteration. The next important issue is how to detect and merge the redundant initial boundaries during the 1-D inversion. We employ the golden section search to merge redundant layers, which is based on the golden section rule. The details can be referred to [15]. Since it is a very mature method, we can omit it here.

2.2.5. Noise Analysis

Different from the other inversions with the white noise, we simulate the real field noise and add it into our inversion in the testing. According to Anderson [16], we incorporate two types of noises: coherent noise and incoherent noise to simulate borehole noise, which is the main source of the noise.

For coherent noise, since the triaxial array is assumed to be co-located, the borehole noise will be correlated in all the measurements. In this case, all coils should have the same noise level. Assume The coherent noise can be written as

$$\text{Noise}_{\text{coherent}}(T_i, R_j) = S \cdot ran \cdot \bar{E}(T_i, R_j) \tag{27}$$

where S is the scale factor, and $\bar{E}(T_i,\ R_j)$ is the mean value of the jth receiver with ith transmitter firing. Note that all the channels employ the same random numbers ran between 0 and 1.

On the other hand, if the x, y, and z coils are not co-located, or if the tool is moving at an irregular speed, the noise will be incoherent. In order to simulate incoherent noise, an array of different random numbers will be generated for each measure channel and then scaled and added as above [16]. The incoherent noise is given by

$$\text{Noise}_{\text{coherent}}(T_i, R_j, k) = S \cdot ran(T_i, R_j, k) \cdot \bar{E}(T_i, R_j, k) \tag{28}$$

Different from (27), the random function $ran(T_i,\ R_j,\ k)$ of (28) is changed versus receiver channel.

3. NUMERICAL RESULTS AND DISCUSSIONS

Based on the above theory, we developed a 1-D inversion code. In this section, we will demonstrate the capability and robustness of the inversion by synthetic data and a field log data. If without specific illustration, in all the examples, initial models are provided by Zero-D inversion. No priori information is required in our inversion procedure. The conductivity σ, dipping angle α, rotation angle γ, and the bed-boundary parameters Z_i are enforced to be within the following range:

$$\begin{aligned} 0.0005 < \sigma < 5 \\ 0.0001 < \alpha < 89^\circ \\ 0.0001 < \gamma < 180^\circ \\ Z_{i-1} < Z_i < Z_{i+1} \quad (2 \le i \le L-2) \\ D_0 < Z_1 < Z_2 \\ Z_{L-2} < Z_{L-1} < D_N \end{aligned}$$

It should be noted that the limits on boundary are dynamic. D_o and D_N are the depth of the first and last measured data, respectively. Hence each layer can shift maximum between the adjacent boundaries. The examples were run on a 2-core 2.61 GHz, 1.87 GB PC.

3.1. Example 1

First, we validate our inversion algorithm using the Oklahoma benchmark model [17]. The formation has 21 layers. The distance between the transmitter and the receiver is 20 inches and the operating frequency is 20 kHz. The dipping angle is 60° and the rotation angle is 0°. The full magnetic responses are provided by a forward modeling based on FEM from the University of Houston [18]. We employ this benchmark model to fully test our inversion algorithm.

We apply the synthetic full matrix, synthetic data with 5% coherent noise and synthetic data with 5% incoherent noise as the input of the inversion, respectively.

Figure 3 shows the real conductivity and the inverted conductivity obtained from the synthetic raw matrix, the contaminated data with 5% coherent noise and 5% incoherent noise. The dashed lines are initial guesses of conductivity from Zero-D inversion. Although redundant initial layers are given, the 1-D inversion still successfully converges and provides reliable inversion results in all the three cases. As shown in Fig. 3, the inverted anisotropic conductivity matches very well with the true values, especially for the synthetic input and 5% incoherent noise.

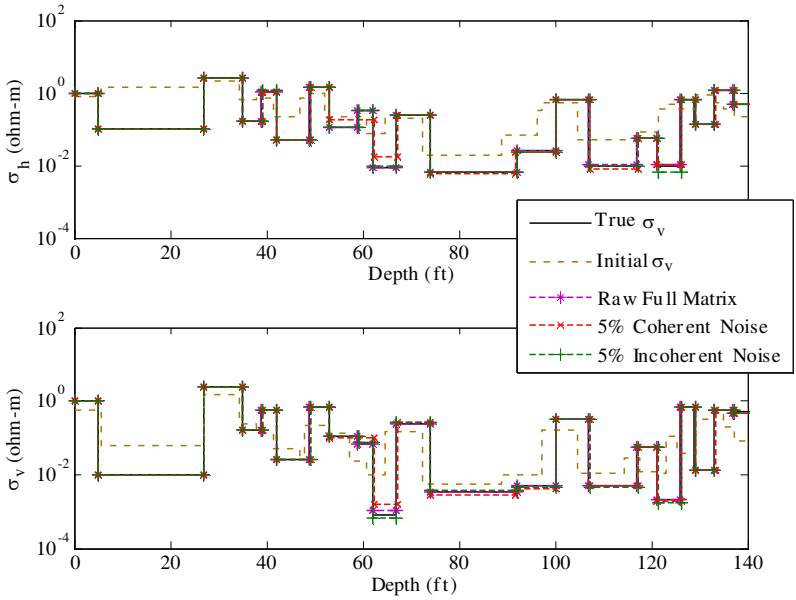

Figure 3. Inverted conductivity with the synthetic raw data for the Oklahoma benchmark model.

Table 1. Initial and inverted dipping angle, rotation angle with different input data.

Angle	Initial Guess	Synthetic Full Matrix	Coherent Noise	Incoherent Noise
$\alpha\,(^\circ)$	60.99	59.99	59.93	59.95
$\gamma\,(^\circ)$	0.005	0.005	0.005	0.005

Table 1 gives the initial guess of the dipping angle, rotation angle and the inverted dipping and rotation angle for each case. The initial guess is obtained by the Zero-D inversion with the synthetic raw data. For all of the three different inputs, the 1-D inversion provides correct dipping angle and rotation angle. Considering Fig. 3, the 1-D inversion is proved to be reliable and meets our expectation which is to develop a reliable inversion algorithm.

In Fig. 4, we show the convergence property of the three cases. It is observed that the cost function with the 5% coherent noise is a slightly higher than the other two cases due to the misfit between the eighth and ninth layer. The inversion with 5% incoherent noise consumes the most

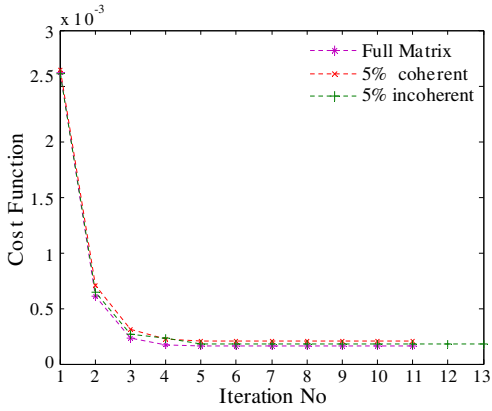

Figure 4. The cost functions versus the iteration number for the three inversion cases.

time. For this multilayer model, the inversion code took about 590, 491 and 650 minutes to obtain the final result under the three cases: uncontaminated raw data, 5% coherent noise and 5% incoherent noise. It is found that the third case cost the most time. Furthermore, we can see from Fig. 3 that the error becomes larger for high resistive layers (the conductivity is smaller than 0.01 S/m). This is reasonable since the induction logging tool has a better sensitivity to the conductive layer than the resistive layer, because the induction current source depends on the formation conductivity. Weak conductivity induces less current and hence gives less contribution to the tool responses. It is well known that when the formation resistivity is larger than 100 ohm-m, the resolution of the induction logging tool significantly decreased. Therefore, it is reasonable that the 1-D inversion has slightly higher misfit on the 10th, 12th, 15th and 17th layers.

According to the inversion results of this benchmark model, the 1-D inversion model works successfully and is demonstrated to be a qualified inversion algorithm.

3.2. Example 2

In the second example, the formation model is a simple three-layer anisotropic model, as shown in Fig. 5. The formation is characterized by a high-resistivity pay zone surrounded by two symmetric isotropic zones.

The synthetic data used in this example are sampled from 10 ft to 50 ft with a 0.25 ft step. We use the triaxial array as shown in Fig. 1

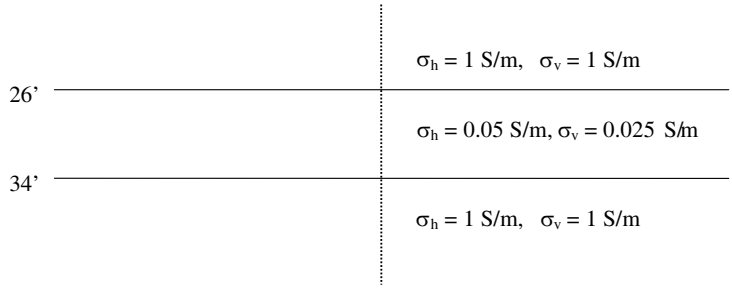

Figure 5. A three-layer anisotropic model.

Table 2. The inverted dipping angle and rotation angle in Validation I.

Validation I	Initial Guess	Full Matrix	Diagonal Matrix
$\alpha\,(^\circ)$	32.29	30.00	30.00
$\gamma\,(^\circ)$	34.63	60.00	120.00

to collect data. The distance between the transmitter and receiver is 40 inches. The working frequency is 20 kHz. In this example, the dipping angle is 30° and the rotation angle is 60°.

We apply the full matrix as well as the diagonal terms of the apparent conductivity tensor as the input log data, respectively. By comparing the inversion results from these two input data, we want to investigate whether reducing input data can still guarantee the accuracy of the 1-D inversion and also improve the inversion speed.

3.2.1. Validation I — Raw Data

We first apply the raw data without noise to do the inversion. The initial guess is provided by the Zero-D inversion with the full matrix.

Figure 6 shows the initial guess and inverted conductivity profile. The maximum relative error of the inverted horizontal and vertical conductivities is less than 0.1%.

Table 2 presents the initial guess and inversion results of the dipping angle, rotation angle obtained from the full matrix and the diagonal terms, respectively. We can see that the inversion results from the full matrix and the diagonal terms match well with the true parameters except the rotation angle given by the diagonal terms is different from the true value. The inverted rotation angle (120°) becomes the coangle of the true rotation angle (60°).

In Fig. 6, we compare the raw data and the calculated responses from the inverted formations. As can be seen, the components σ_{xx},

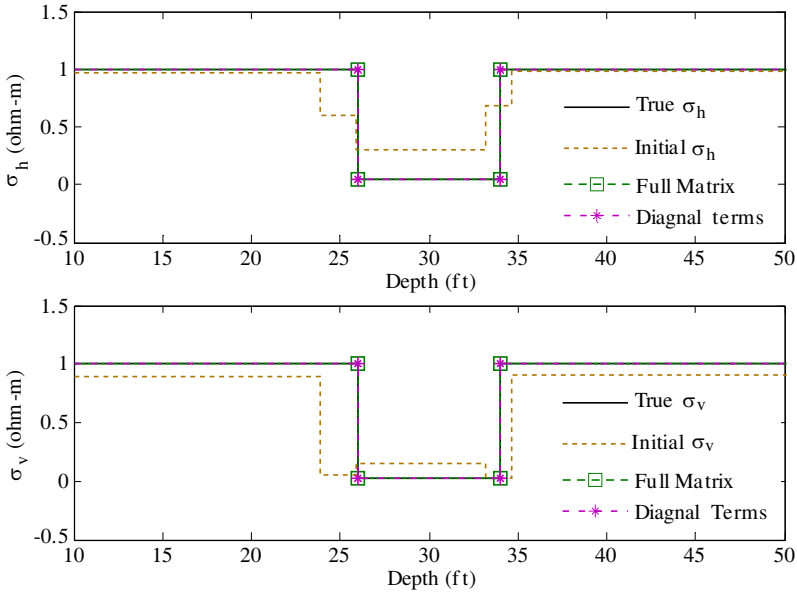

Figure 6. Inverted conductivity profile with the synthetic raw data for the model in Fig. 5. The true dipping angle and rotation angle are 30° and 60°, respectively. The solid black line represents true anisotropic resistivity. The initial guess is shown by the gray dotted line. The green dashed line with square mark represents the inverted results using the full resistivity matrix. The purple dashed line with star mark represents the inverted result using the diagonal terms.

Table 3. The CPU time cost in Validation I.

Inversion model	Full Matrix	Diagonal Matrix
Time (s)	92	106

σ_{yy}, σ_{zz}, σ_{yz}, and σ_{zy} from the inverted formation obtained both the full matrix and diagonal terms coincide with the raw data. However the cross components σ_{xz}, σ_{xz}, σ_{yz} and σ_{zy} obtained from the diagonal term inversion model are exactly in the reverse direction of the raw log since the inverted rotation angle is the coangle of the true one. Thus we can conclude that eliminating the cross components in inversion will introduce uncertainty when determining the rotation angle.

Table 3 shows the total CPU time cost by the inversions using the full conductivity matrix and the diagonal terms, respectively. We can see that the when using the full matrix to do the inversion, the procedure converges faster and cost less time. In Fig. 7 we compare

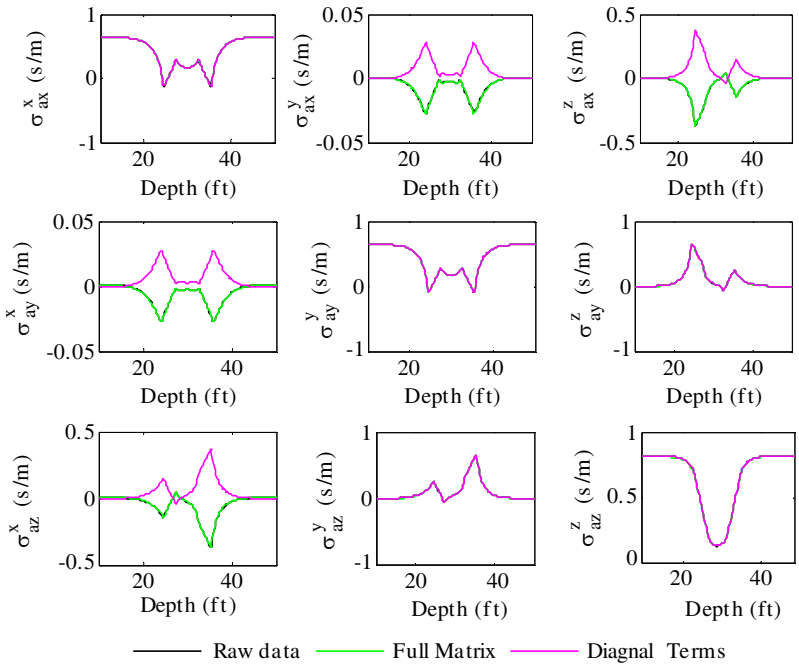

Figure 7. Comparison of the apparent conductivity simulated from the two inverted model and the raw data.

the cost functions of the two inversion models versus the iteration numbers. Compared with the full-matrix model, the diagonal-term model requires more iteration to converge. As a result, the diagonal-term model still yields slower behavior than the full-matrix model even the iteration costs less computational time.

Based on above analysis, we can conclude that eliminating the cross components cannot bring any benefit on the inversion speed as well as efficiency. As we discussed, only replying on the diagonal-term model will introduce uncertain effect on the rotation angle and slow down the inversion speed.

3.2.2. Validation II — 5% Coherent Noise

Next, we add 5% coherent noise to the raw data and repeat the inversion procedure. Table 4 presents the initial guess and inversion results of the dipping angle and the rotation angle, which presents accurate angles. Table 5 shows the cost time. Fig. 9 compares the inverted conductivity with the true parameters. Very good agreement is observed. The maximum error of the inverted horizontal and vertical conductivity is about 3%.

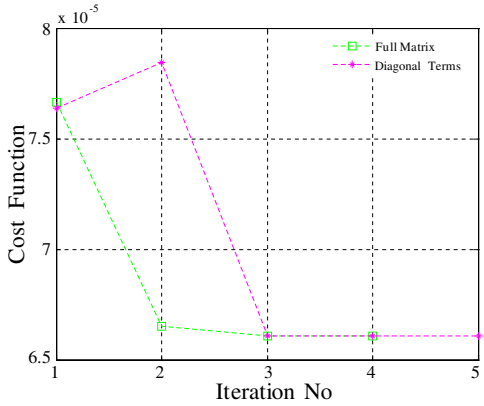

Figure 8. The cost function of the two inversion models versus the number of iterations.

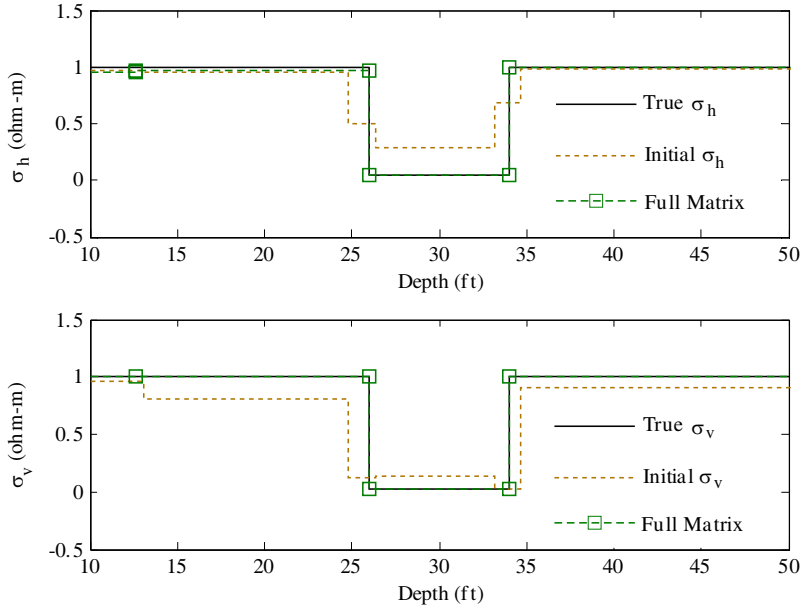

Figure 9. Inverted conductivity obtained from the synthetic data for the model in Fig. 5 with the input log contaminated by 5% coherent noise.

3.2.3. Validation III — 5% Incoherent Noise

Next, we add 5% incoherent noise to the input log data and repeat the inversion. Fig. 10 presents the inverted horizontal and vertical conductivities. The maximum relative error of the inverted horizontal

Table 4. The inverted dipping angle and rotation angle in Validations II & III.

Validation I	Initial Guess	Validation II	Validation III
α (°)	30.53	30.16°	30.5°
γ (°)	27.54	60.04°	59.33°

Table 5. The CPU time cost in Validations II & III.

Inversion model	5% Coherent (II)	5% Incoherent (III)
Time (s)	220	508

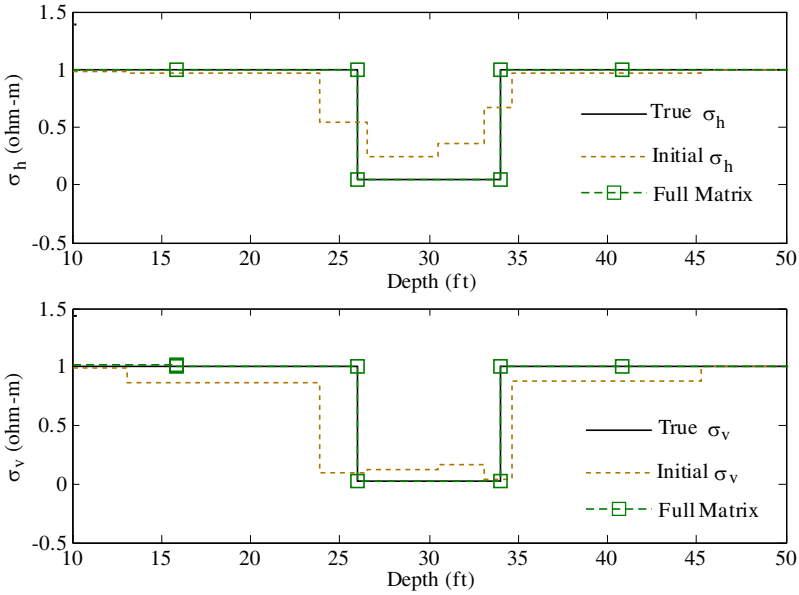

Figure 10. Inverted conductivity obtained from the synthetic data for the model in Fig. 5 with the input log contaminated by 5% incoherent noise.

and vertical conductivities is about 8%. From Fig. 10, we can see that the presence of the incoherent noise cause a stronger negative impact on the Zero-D inversion than the coherent noise and more layers are generated in the initial guess. However, the inversion still yields satisfactory results despite the bad initial guess.

4. CONCLUSION

In this paper, we presented an inversion algorithm for triaxial induction logging in 1-D layered transverse isotropic formation. The Gauss-Newton algorithm is employed to modify Newton step from Gauss-Newton algorithm and thus reduces the cost function. In order to improve the effectiveness of the Gauss-Newton algorithm, Gill and Murray Cholesky factorization is used to calculate the Hessian matrix in the quadratic model of the cost function. Zero-D inversion is used to generate the initial guess. In order to obtain good initial guess, both the variance-based method and the horn effect of the cross components are used to determine the initial boundary. Then golden section search is applied to merge redundant initial boundaries during the inversion. The resultant inversion algorithm was validated by synthetic data from our forward modeling and other different forward modeling. Satisfactory inversion results can be obtained in various cases despite of the noise. We also demonstrate the capability of our code in the application of the real field log inversion.

ACKNOWLEDGMENT

Manuscript received August 10, 2012. This work was supported in part by Well Logging Laboratory, University of Houston.

REFERENCES

1. Weiss, C. J. and G. A. Newman, "Electromagnetic induction in a fully 3-D anisotropic earth," *Geophysics*, Vol. 67, No. 4, 1104–1114, Jul. 2002.
2. Abubakar, A., T. M. Habashy, V. Druskin, L. Knizhnerman, and S. Davydycheva, "A 3D parametric inversion algorithm for tri-axial induction data," *Geophysics*, Vol. 71, No. 1, G1–G9, Jan. 2006.
3. Cheryauka, A. B. and M. S. Zhdanov, "Fast modeling of a tensor induction logging response in a horizontal well in inhomogeneous anisotropic formations," *SPWLA 42nd Annual Logging Symposium*, Jun. 2001.
4. Yu, L., B. Kriegshauser, O. Fanini, and J. Xiao, "A fast inversion method for multicomponent induction log data," *71st Annual International Meeting, SEG, Expanded Abstracts*, 361–364, 2001.
5. Lu, X. and D. Alumbaugh, "One-dimensional inversion of three

component induction logging in anisotropic media," *71st Annual International Meeting, SEG, Expanded Abstracts*, 376–380, 2001.

6. Zhang, Z., L. Yu, B. Kriegshauser, and L. Tabarovsky, "Determination of relative angles and anisotropic resistivity using multicomponent induction logging data," *Geophysics*, Vol. 69, 898–908, Jul. 2004.
7. Wang, H., T. Barber, R. Rosthal, J. Tabanou, B. Anderson, and T. M. Habashy, "Fast and rigorous inversion of triaxial induction logging data to determine formation resistivity anisotropy, bed boundary position, relative dip and azimuth angles," *73rd Annual International Meeting, SEG, Expanded Abstracts*, 514–517, 2003.
8. Abubakar, A., P. M. van den Berg, and S.Y. Semenov, "Two- and three-dimensional algorithms for microwave imaging and inverse scattering," *Journal of Electromagnetic Waves and Applications*, Vol. 17, No. 2, 209–231, 2003.
9. Davydycheva, S., V. Druskin, and T. M. Habashy, "An efficient finite-difference scheme for electromagnetic logging in 3D anisotropic inhomogeneous media" *Geophysics*, Vol. 68, 1525–1536, Sep. 2003.
10. Habashy, T. M. and A. Abubakar, "A general framework for constraint minimization for the inversion of electromagnetic measurements," *Progress In Electromagnetic Research*, Vol. 46, 265–312, 2004.
11. Zhong, L. L., J. Ling, A. Bhardwaj, S. C. Liang, and R. C. Liu, "Computation of triaxial induction logging tools in layered anisotropic dipping formations," *IEEE Trans. on Geosci. Remote Sens.*, Vol. 46, No. 4, 1148–1163, Mar. 2008.
12. Wang, H. M., S. Davydycheva, J. J. Zhou, M. Frey, T. Barber, A. Abubakar, and T. Habashy, "Sensitivity study and inversion of the fully-triaxial induction logging in cross-bedded anisotropic formation," *SEG Las Vegas 2008 Annual Meeting*, 284–288, University of Houston, 2008.
13. Gill, P. E. and W. Murray, "Newton-type methods for unconstrained and linearly constrained optimization," *Mathematical Programming*, No. 28, 311–350, Jul. 1974.
14. Zhdanov, M., D. Kennedy, and E. Peksen, "Foundations of tensor induction well-logging," *Petrophysics*, Vol. 42, 588–610, 2001.
15. Hans, W., "The golden section. Peter hilton trans," *The Mathematical Association of America*, 2001.
16. Anderson, B. I., T. D. Barber, and T. M. Habashy, "The interpretation and inversion of fully triaxial induction data; a

sensitivity study," *SPWLA 43rd Annual Logging Symposium*, 2002.

17. Rosthal, R., T. Barber, and S. Bonner, "Field test results of an experimental fully-triaxial induction tool," *SPWLA 44th Annual Logging Symposium*, 2003.
18. Yuan, N., X. C. Nie, and R. Liu, "Improvement of 1-D simulation codes for induction, MWD and triaxial tools in Multi-layered dipping beds," *Well Logging Laboratory Technical Report*, 32–71, Oct. 2010.